Magnetic and electrical transport properties of $La_{0.67}Ca_{0.33}MnO_3$ (LCMO):*x*ZnO composites

2004 J. Phys.: Condens. Matter 16 4089

(http://iopscience.iop.org/0953-8984/16/23/024)

INSTITUTE OF PHYSICS PUBLISHING JOURNAL OF PHYSICS: CONDENSED MATTER

J. Phys.: Condens. Matter **16** (2004) 4089–4102 PII: S0953-8984(04)71657-4

Magnetic and electrical transport properties of $La_{0.67}Ca_{0.33}MnO_3$ (LCMO):xZnO composites

D Das[1], C M Srivastava[2], D Bahadur[1], A K Nigam[3] and S K Malik[3]

[1] Department of Metallurgical Engineering and Materials Science, IIT Bombay, India
[2] Department of Physics, IIT Bombay, India
[3] Tata Institute of Fundamental Research, Colaba, Mumbai 400005, India

Received 10 November 2003, in final form 19 January 2004
Published 28 May 2004
Online at stacks.iop.org/JPhysCM/16/4089
DOI: 10.1088/0953-8984/16/23/024

Abstract

We have synthesized $La_{0.67}Ca_{0.33}MnO_3$ (LCMO):xZnO ($0 \leqslant x \leqslant 0.475$) composites through a citrate gel route and have characterized them for magnetic and magnetotransport properties. In lower concentrations ($x \leqslant 0.13$), ZnO mostly goes into the perovskite lattice substituting Mn in LCMO and segregates less in the grain boundary region, but at higher concentration ($x > 0.13$) it segregates mostly at the grain boundaries of LCMO and influences the transport properties significantly. A model is proposed which describes the overall resistivity of the system as a parallel combination of a low resistive intragrain conducting path and a high resistive intergrain insulating path. Using this approach, the grain and grain boundary contributions to the overall resistivity are separated for all the composites. The field dependent resistivity shows that all the composites have higher values of MR at the transition temperatures (T_{MI}) compared to that in pure LCMO ($x = 0$). The highest value of MR is obtained for $x = 0.10$ and is 76.6% at 80 kOe field near T_{MI}.

1. Introduction

Perovskite manganites have been the subject of intense research in the last few years because of their inherent potential to exhibit a wide variety of interesting physical properties which include colossal magnetoresistance (CMR) [1]. The work of Jin *et al* [2] triggered extensive research in this fascinating field. The CMR effect, caused by the 'double exchange' mechanism, proposed by Zener [3] in 1951, is useful to mostly explain the intrinsic CMR within the grains. CMR related to extrinsic effects, on the other hand, is largely dependent on the grain boundary properties and is generally ascribed to the spin polarized intergrain tunnelling of conduction electrons [4]. Since the tunnelling process takes place across the interfaces or grains separated by an energy barrier (related to the magnetic disorder [5]), dilution with secondary phases in the manganites, which impede the magnetic homogeneity near the grain boundary area,

will adjust the barrier layer and, hence, influence the tunnelling process. Also, since these extraneous effects act as pinning centres in remagnetization by domain wall displacement [6], a small field will align the neighbouring ferromagnetic (FM) grains and hence an enhanced magnetoresistance (MR) response can be achieved at low fields and at low temperatures. This extrinsic effect is observed in a wide temperature range and at low fields ($H \leqslant 1$ kOe) and makes it more useful from an application point of view.

Although spin-polarized tunnelling through the grain boundaries leads to high MR at low fields at a composition called the percolation threshold for the composite system, its magnitude falls off rapidly with temperature. Several workers have attempted to enhance the low temperature low field MR (LFMR) or the room temperature MR by making composites of these CMR oxides like $La_{0.67}Ca_{0.33}MnO_3$ (LCMO) or $La_{0.67}Sr_{0.33}MnO_3$ (LSMO) with secondary phases such as an insulating oxide [7–11], a hard ferromagnetic material [12], a soft magnetic material [13], a polymer material [14], a glass [15], a metal [16] or metal oxide [17] or with other CMR oxides [18, 19]. But in every case the basic objective is to increase the height of the tunnel barrier between the neighbouring FM grains. Awana *et al* [20] have studied the effect of Zn substitution on the magnetic transition temperature in $La_{0.67}Ca_{0.33}Mn_{1-x}Zn_xO_3$ for $x = 0.0$–0.50. Although they have carried out structural, magnetic and thermal measurements for the entire range, they did not report the transport measurements on these. The present investigation is an attempt to increase the MR of magnetoresistive LCMO through the formation of a composite with ZnO. Since ZnO is a semiconducting material, it should affect the electrical transport of the composites. We have performed room temperature powder diffraction to confirm the phase formation. Magnetization (M versus T) and electrical resistivity (ρ versus T) measurements have been carried out with and without magnetic field to characterize the magnetotransport properties of these composites. A correlated polaron hopping model has been used to analyse the transport data that gives a satisfactory fit with the experimental data throughout the temperature range studied by us, and the results are presented in this paper.

2. Experimental details

A standard citrate-gel route has been used to synthesize $La_{0.67}Ca_{0.33}MnO_3$ (LCMO):xZnO ($x = 0.0$–0.475) composites [10]. Stoichiometric amounts of La_2O_3, $CaCO_3$, $MnCO_3$ and ZnO (all Aldrich Chemical with purity more than 99.5%) were first converted to aqueous nitrate by the addition of concentrated HNO_3, where $MnCO_3$ was precipitated as insoluble black MnO_2. The addition of citric acid dissolved the insoluble residue leading to the formation of a cation–citric acid complex. Ethylene glycol was then added to this cationic complex. Vigorous stirring of this resulting sol solution for 1–2 h, followed by heating at around 90 °C for several hours, led to the formation of a brown transparent gel. On further heat treatment of the gel at about 150 °C, a fluffy dried mass was obtained. The precursor powder so obtained on calcining at 800 °C for 2 h in air resulted in the formation of the desired phase. The final sintering of the pressed rectangular pellets was done at 1200 °C for 2 h in static air.

Room temperature powder x-ray diffraction (XRD) patterns of the samples were recorded with a Philips PW 1729 diffractometer in the 2θ range 20°–80° with a step size of 0.050 using Cu Kα radiation. A microstructural study was done using an environmental scanning electron microscope (ESEM model SEI QUANTA 200). Magnetization measurements were carried out using a vibrating sample magnetometer (Oxford VSM) in the temperature range 4–300 K. The temperature dependence of electrical resistivity ($\rho(T)$) was measured by a standard four probe dc technique in a quantum design PPMS (model 6000) in the temperature range of 4–320 K. The magnetic field dependence of resistivity was measured in a field of 80 kOe in the same temperature range.

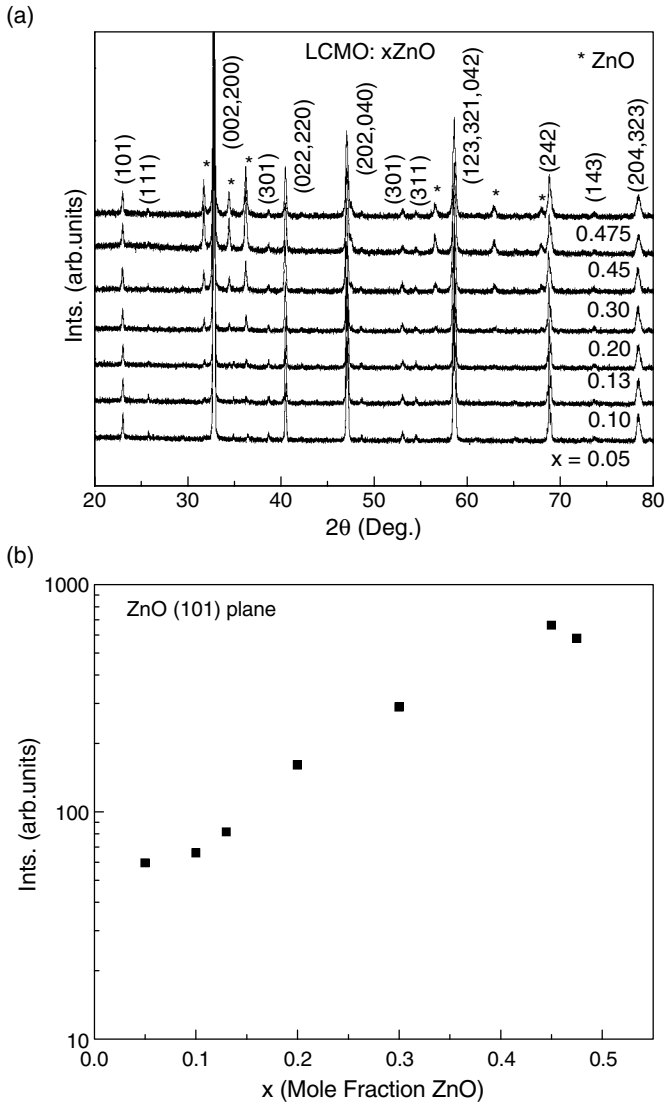

Figure 1. (a) Room temperature powder x-ray diffraction patterns of LCMO:xZnO ($0 \leqslant x \leqslant 0.475$) composites. (b) Intensity of the strongest peak (101) of the ZnO phase with composition, x, for the LCMO:xZnO ($0 \leqslant x \leqslant 0.475$) composites.

3. Results and discussions

The XRD patterns of the composites LCMO:xZnO are shown in figure 1(a). In lower concentrations ($x \leqslant 0.13$) ZnO mostly goes into the perovskite lattice substituting Mn in LCMO and segregates less in the grain boundary region, but at higher concentration ($x > 0.13$) it segregates mostly at the grain boundaries of LCMO. The intensity of the ZnO lines increases with composition, x. The logarithmic intensity of the strongest peak (101) of the ZnO phase has been plotted against composition, x, in figure 1(b). There is a clear change in the slope, d(Ints.)/dx, near $x = 0.13$, indicating the segregation of ZnO in the grain boundary region

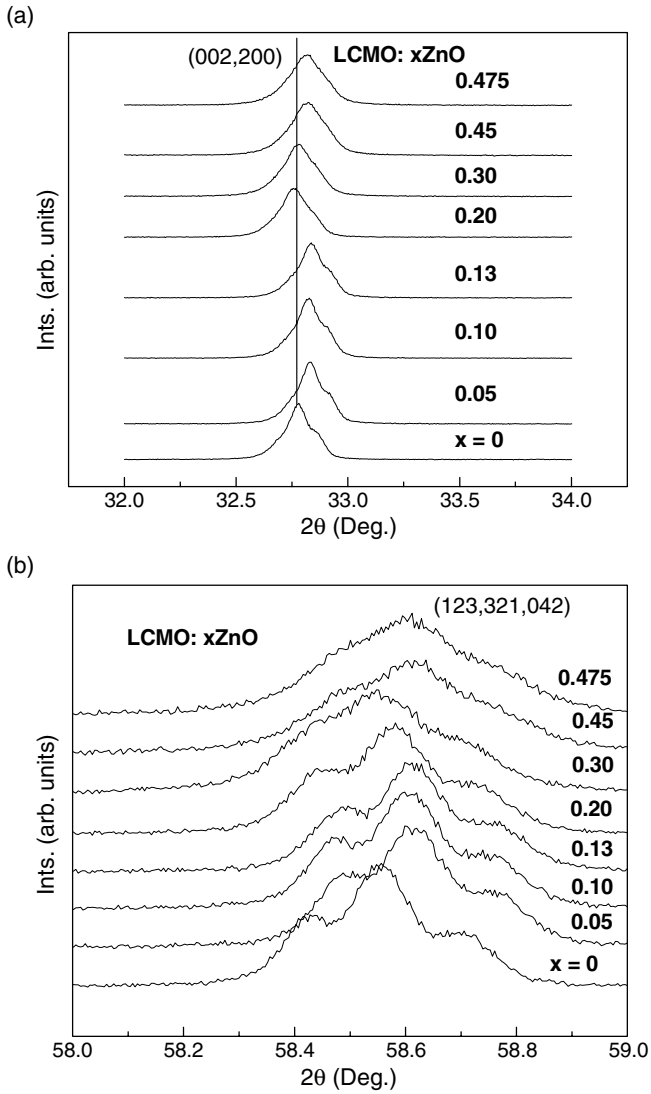

Figure 2. (a) Shifting of the most intense line (002, 200) and change in crystal symmetry of LCMO:xZnO composites. The vertical line is a guide to the eye. (b) Shifting of the second intense line (123, 321, 042) and change in crystal symmetry of LCMO:xZnO composites.

for $x \geqslant 0.13$. Awana *et al* [20] have, however, observed an isostructural substitution of Zn at the Mn site up to $x = 0.30$. Beyond this value of x, they observed some extra lines, which they have attributed to the presence of ZnO in the system as a separate phase. As discussed below, this is also true for the present system. Lattice parameters of the orthorhombic LCMO in the composite system have been calculated by a least-squares fitting of the observed 2θ (or d) values in the x-ray powder diffraction data and are given in table 1. The variation in lattice parameters does not show any regular trend. The crystal symmetry changes from orthorhombic to cubic in the presence of Zn in the LCMO matrix, which becomes prominent for $x \geqslant 0.30$. Shifting of the two most intense lines (002, 200) and (123, 321, 042) along with the gradual change in crystal symmetry is shown in figures 2(a) and (b), respectively.

Table 1. Variation of lattice parameters and unit cell volume with composition, x, for LCMO: xZnO composites.

LCMO:xZnO (x)	a (Å)	b (Å)	c (Å)	Cell volume (Å^3)
0	5.46	7.71	5.47	230.29
0.05	5.45	7.70	5.47	229.49
0.10	5.45	7.70	5.46	229.28
0.13	5.45	7.70	5.46	229.03
0.20	5.45	7.71	5.47	229.59
0.30	5.46	7.72	5.46	230.02
0.45	5.45	7.72	5.46	229.46
0.475	5.45	7.71	5.46	229.35

Table 2. Magnetization and electrical transport parameters of the LCMO:xZnO composites obtained from the experiment.

x	T_C (K)	M_S (emu g^{-1})	T_{MI} (K)	ρ_{MI} (Ω cm)	Peak MR (%)
0.0	264	91.6	260	0.45	59
0.05	240	90.8	232	2.94	68
0.10	227	86.4	217	24.24	77
0.13	226	84.0	217	37.37	67
0.20	223	82.3	222	0.97	73
0.30	225	78.6	220	3.29	76
0.45	229	67.0	211	5.03	—
0.475	235	65.2	205	40.93	—

Scanning electron micrographs (figures 3(a)–(c)) along with an EDX analysis of the thermally etched surface of the composite samples show uniform distribution of ZnO throughout the matrix for lower concentration of ZnO. But ZnO gets segregated for higher concentration ($x \geqslant 0.13$). The microstructures show uniform compaction with varying particle size of the order of 1–2 μm and even less. For low concentrations of ZnO ($x \leqslant 0.10$), Zn enters the LCMO lattice and hence the entire matrix shows the presence of Zn. Also, for $x = 0.10$, refined smaller grains with better size distribution are seen. ZnO appears to work as a sintering aid. As x increases, Zn segregates as a separate phase (ZnO) in the LCMO matrix, which is seen as brighter spots in the microstructure. Also with increasing x, the cluster sizes of ZnO increase ensuring better interparticle contact between LCMO grains. An EDX analysis with spot scan of the micrographs indicates that for smaller x, ZnO tends to go to the lattice. As x increases, more and more Zn diffuses from the interior of the LCMO grains and gets segregated in the grain boundaries. So ZnO cluster sizes increase with increasing x, as seen in the micrographs. The higher wt% of Zn (for samples with higher x values) is seen as brighter spots in figure 3(c).

The temperature (T) dependence of magnetization (M) has been measured in an applied field of 5 kOe for all the composites and the results are shown in figure 4. If all Mn^{3+} and Mn^{4+} spins are aligned parallel due to double exchange, the saturation magnetization, M_S, value expected for pure LCMO, $x = 0.0$, would be approximately 98 emu g^{-1} (assuming a spin only moment), which is about 6% higher than the value measured in our pure LCMO sample. The magnetic data on all the composites are given in table 2. The value of M_S for our pure compound ($x = 0$) agrees well with that reported in the literature [21]. Saturation magnetization decreases with x as expected, due to the decrease in the volume fraction of the LCMO phase and increase of the nonmagnetic ZnO phase in these composites. The variation

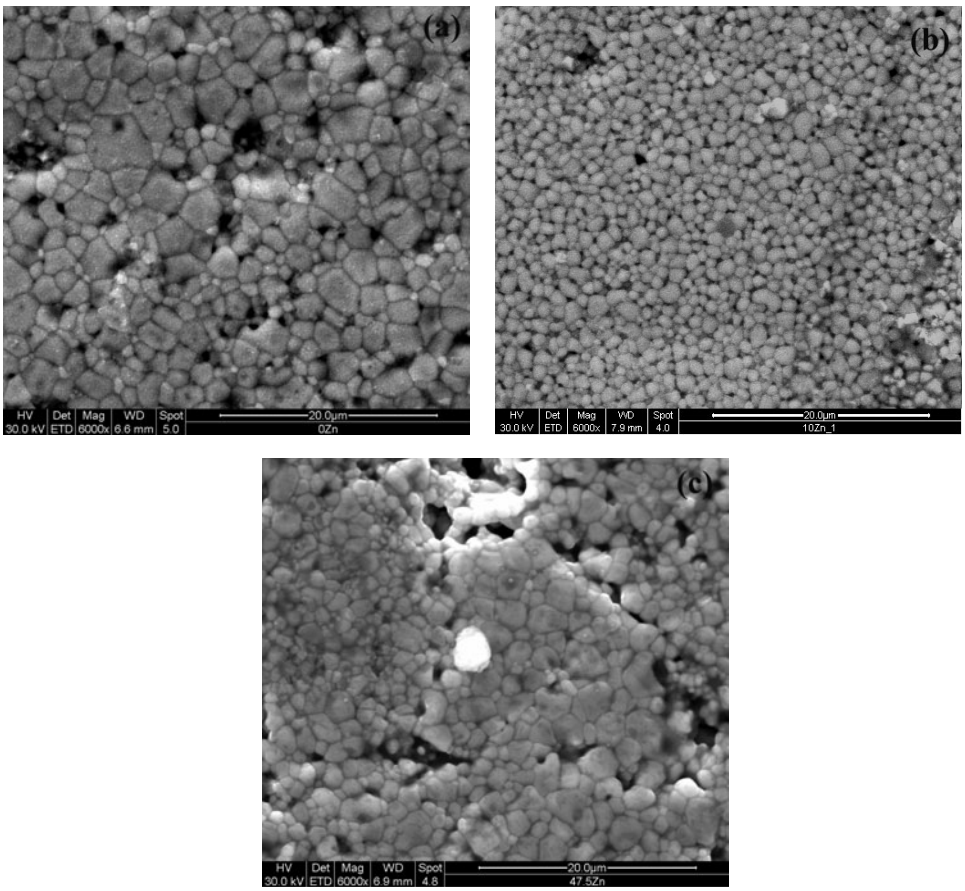

Figure 3. Scanning electron micrographs of LCMO:xZnO samples with (a) $x = 0.0$, (b) $x = 0.10$, and (c) $x = 0.475$. The bright spots in figure 3(c) correspond to Zn rich areas.

of saturation magnetization at 5 K with composition (x) is shown in the inset (a) of figure 4. All the composites show similar M–T behaviour as the pure LCMO sample. All of them show a sharp ferromagnetic to paramagnetic transition indicating magnetic homogeneity of our samples. The Curie temperature, T_C, obtained as the maximum inflection of the M–T curve, shifts from 264 K for $x = 0.0$ to 240 K for $x = 0.05$ and further goes down to 227 K for $x = 0.10$ and then remains essentially constant thereafter for $x \geqslant 0.13$. This suggests that up to 10 mol% of ZnO, Zn has gone into the lattice substituting Mn and after that it is segregated at the grain boundary, as also suggested by Ghosh *et al* [22] in their transition element doped LCMO. The variation of T_C with composition, x, is shown in the inset (b) of figure 4. Awana *et al* [20] have also observed a decrease in T_C with x and the rate of fall (dT_C/dx) is smaller for lower x (up to $x = 0.075$) than at higher concentrations of Zn. They find a reduction of T_C from 277 K for $x = 0.0$ to 185 K for $x = 0.15$. But for $x > 0.15$ they could not trace T_C clearly. In our present work, we have observed a distinct paramagnetic to ferromagnetic transition in all the samples and the T_C values for all of them are given in table 2.

The resistivity versus temperature behaviour of the composites is shown in figure 5 in the temperature range 5–320 K. The room temperature zero field resistivity of the samples increases with x up to $x = 0.13$ as shown in figure 6, and thereafter it decreases as x increases further. All the composites show metal–insulator transition, close to their ferromagnetic transition

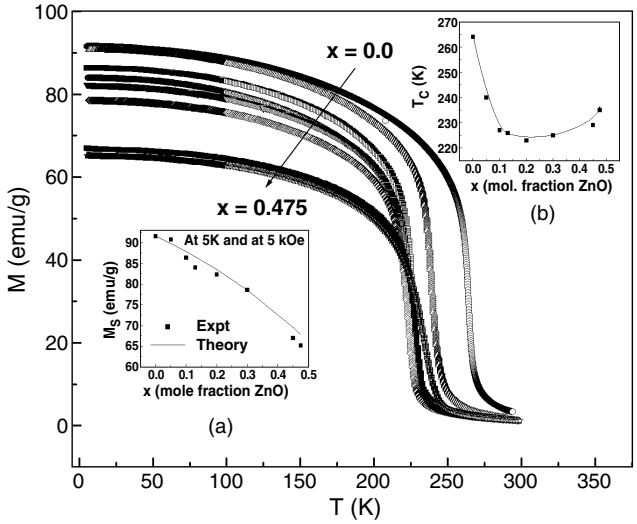

Figure 4. Plot of magnetization (in 5 kOe field) versus temperature for the LCMO:xZnO composites. Inset (a): variation of the saturation magnetization at 5 K with composition (x) from the experimental data and the calculated moment based on the magnetic LCMO fraction only. Inset (b): variation of T_C with composition, x, in LCMO:xZnO composites.

temperature, which shifts from 262 K for $x = 0.0$ to 216 K for $x = 0.10$ and then remains constant at around 217 K for the other composites. The room temperature or the peak resistivity at T_{MI} does not increase as much as is observed in the case of LCMO:$x$$SiO_2$ composites studied earlier [10]. The variation of room temperature resistivity with composition (x), shown in figure 6, indicates an approximately two orders of magnitude increase in resistivity for the $x = 0.13$ sample compared to that of pure LCMO, but no percolation limit is observed in this case. If Zn substitutes Mn in the perovskite lattice, being a diamagnetic ion, it cannot participate in the double exchange (DE) mechanism involving Mn^{3+} and Mn^{4+} ions through the Mn^{3+}–O–Mn^{4+} network, so, in effect, it dilutes the DE process and hence the resistivity increases initially up to $x = 0.13$. Also Zn^{2+} at the Mn site, being a bigger ion, should compress some Mn^{3+}–O–Mn^{+4} bonds which in turn should lead to bond angle distortion ($<180°$) and will result in a reduction of the mobility of the charge carriers as suggested by Ghosh *et al* [22]. But since Zn^{2+} cannot acquire a higher valent state, it induces a higher residence time of the higher valent Mn ion, namely Mn^{+4}, in its close vicinity thereby causing a local charge ordering. The local charge ordering in turn would straighten out some Mn^{3+}–O–Mn^{4+} bonds in its immediate neighbourhood and will make the Mn^{+3}–O–Mn^{4+} angle close to 180°, releasing strain in the system which will lead to the improved mobility of the charge carriers [22]. This effect becomes prominent for $x \geqslant 0.20$.

To discuss the variation of room temperature resistivity with composition, the following model is proposed. The overall transport of the system can be discussed in terms of a combination of intragrain and intergrain hopping of the conduction electrons between the neighbouring sites. As the overall transport is governed both by low resistive intragrain and high resistive intergrain conduction, the equivalent resistivity of the system is a parallel combination of grain (ρ_g) and grain boundary (ρ_{gb}) as shown schematically in figure 7. The equivalent resistivity, ρ can be expressed as

$$\frac{1}{\rho} = \frac{1}{\rho_g} + \frac{1}{\rho_{gb}}. \tag{1}$$

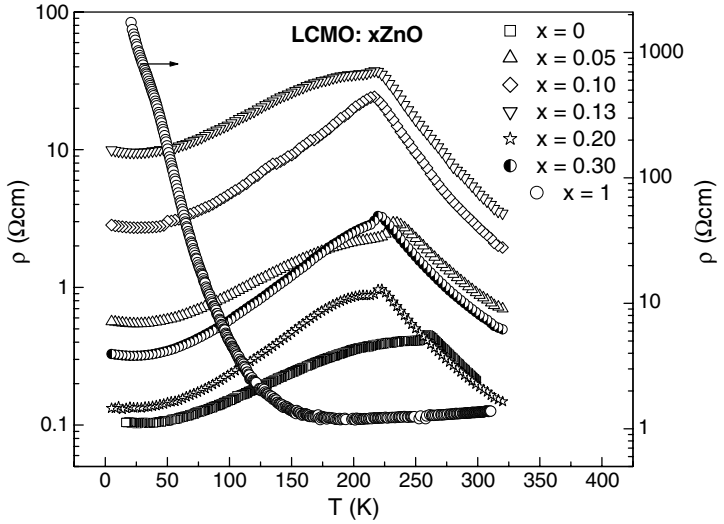

Figure 5. Zero field resistivity behaviour of the LCMO:xZnO composites with temperature. Resistivity behaviour of pure ZnO ($x = 1$) with temperature is also shown (right hand Y axis scale).

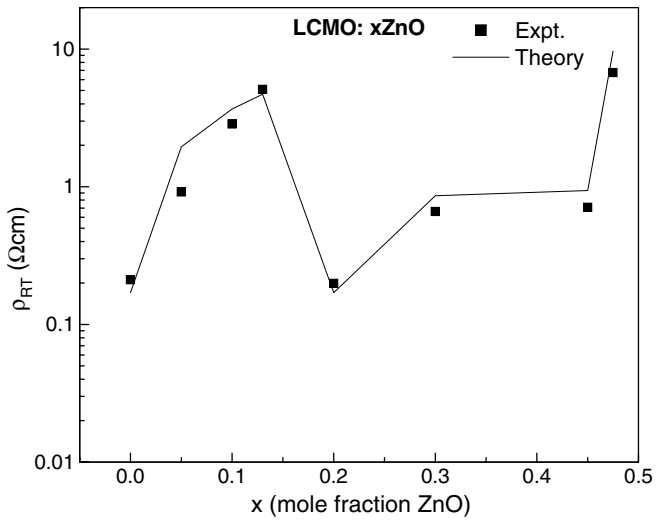

Figure 6. Room temperature resistivity variation of the LCMO:xZnO composites with composition (x). The solid line is the theoretical fit based on the model proposed in the text.

The resistivity of ZnO is more than that of pure LCMO throughout the temperature range studied. Moreover, due to the disordered nature of the grain boundaries, grain boundary resistance is more than the resistance inside the grains. Zn behaves differently at different concentrations. At low concentrations, in the range, $0 \leqslant x \leqslant 0.13$, much of the Zn goes inside the grains substituting Mn in the LCMO lattice and less of it (ZnO) goes to the grain boundary region which is not seen as a separate phase, as shown in figure 3(b). In this composition range, as x increases both ZnO within the grain and grain boundary increases such that the

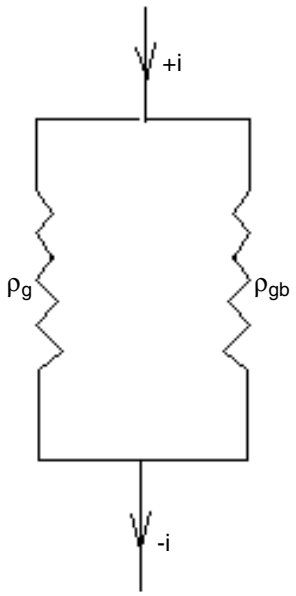

Figure 7. Circuit model of the grain and grain boundary conduction in a LCMO:xZnO composite system.

contribution of grain and grain boundary to total resistivity can be expressed as

$$\rho_{\mathrm{g}}\ (\Omega\ \mathrm{cm}) = 0.2 + \alpha x \tag{2}$$

$$\rho_{\mathrm{gb}}\ (\Omega\ \mathrm{cm}) = 1 + \beta x \tag{3}$$

where α and β are the coefficients which determine the grain and grain boundary contributions, respectively, to the total resistivity of the system and x is the ZnO concentration. Above $x = 0.13$, the resistivity of the composite suddenly falls to that of pure LCMO. The concentration at which this fall occurs may be considered as the critical concentration, x_{c} (=0.20). At higher concentrations, $x > 0.13$, much of the ZnO goes in the grain boundary and less goes inside the grain. Microstructural studies support this observation. In the range $0.13 \leqslant x \leqslant 0.45$, since ZnO goes out of the grains and segregates in the grain boundary region, it improves the interparticle contact inside the grains. In this range the overall resistivity is much more dependent on the grain resistivity than on grain boundary resistivity. In this region the grain and grain boundary resistivity can be expressed as

$$\rho_{\mathrm{g}}\ (\Omega\ \mathrm{cm}) = 0.2 + \alpha(x - x_{\mathrm{c}}) \tag{4}$$

$$\rho_{\mathrm{gb}}\ (\Omega\ \mathrm{cm}) = 1. \tag{5}$$

However, beyond $x = 0.45$, the overall transport is governed mostly by the grain boundary contribution. For $x > 0.45$, the grain and grain boundary resistivity can be taken as

$$\rho_{\mathrm{g}}\ (\Omega\ \mathrm{cm}) = 0.2 + \alpha(x - x_{\mathrm{c}}) \tag{6}$$

$$\rho_{\mathrm{gb}}\ (\Omega\ \mathrm{cm}) = 1 + \beta(x - x_{\mathrm{c}}). \tag{7}$$

To fit our room temperature resistivity data we have taken $\alpha = 60\ \Omega$ cm mol^{-1} fraction ZnO and $\beta = 80\ \Omega$ cm mol^{-1} fraction ZnO in the whole composition range studied, $0 \leqslant x \leqslant 0.475$. With these values of α and β, and using equation (1), we have fitted the room temperature resistivity data, and the fit is shown in figure 6 as a solid line. There is good agreement with the experimental data throughout the whole composition range studied by us.

The temperature dependence of MR, measured in 80 kOe field (figure 8), shows a peak near magnetic transition temperature which is caused by the intrinsic CMR effect. The MR

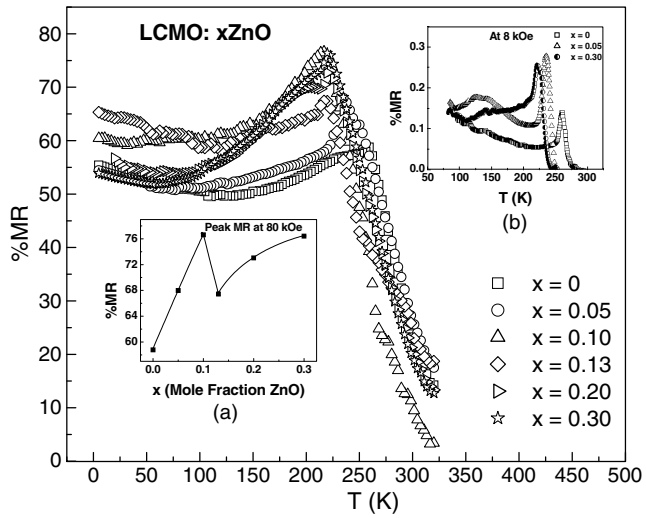

Figure 8. MR behaviour of the LCMO:xZnO composites with temperature. Inset (a) shows the variation of the peak MR measured in 80 kOe field with composition x. Inset (b): the low field MR behaviour of the composites at 8 kOe field and in the temperature range 80–300 K.

behaviour below the transition temperature is interesting and is the manifestation of the extrinsic CMR effect in the system. It shows a high value of around 60% for all the composites and does not depend much on temperature below T_{MI}. This weak temperature dependence of MR is also observed in other CMR composites [8, 11] and has been explained on the basis of spin dependent scattering at the grain boundaries. The enhancement of MR and its near constancy at low temperatures can be ascribed to the magnetically disordered regions near the grain boundary. Because of the secondary phases, the separation between conducting LCMO grains may become comparable to spin memory length [15]. If the effect is only due to the magnetically disordered region near the grain boundary, spin dependent scattering could be essentially responsible for high MR and its near temperature independence below T_{MI}. All the composites show higher values of MR near T_{MI} compared to that in pure LCMO and MR is highest (76.6%) for $x = 0.10$ compared to 58.8% for the pure compound ($x = 0$). The MR values of all the composites are shown in table 2. The variation of peak MR at the transition temperature with composition (x) (displayed in the inset (a) of figure 8) shows a similar trend to that of the room temperature resistivity variation with x shown in figure 6. The low field MR behaviour is particularly interesting in the case of CMR composites. To see the low field grain boundary magnetoresistance we have measured the temperature dependence of MR at 8 kOe field and the variation is shown in the inset (b) of figure 8 for some selected compositions ($x = 0$, 0.05 and 0.30). It is interesting to note that all the composites show higher magnitude of MR compared to pure LCMO at 8 kOe field and for $x = 0.05$ the peak MR is 29% which is almost double that of pure LCMO (15%). So the CMR related to the extrinsic effect [23, 24] is more pronounced in the low field magnetoresistance (LFMR) behaviour of the composites.

We now attempt to analyse the transport results (ρ versus T) discussed above. The resistivity data have been examined using the correlated small-polaron hopping model discussed by one of the authors elsewhere [25]. In this model, the expression for resistivity is given by

$$\rho_{\mathrm{hop}} = \frac{AT}{n}\left[1 + \left\{1 - c'm^2\,(t)\right\}\sigma_{\mathrm{a}}^2\right]\cosh^2\left(\frac{\varepsilon_{\mathrm{p}}}{2\,(T+\theta)}\right)\exp\left(\frac{U}{T}\right) \tag{8}$$

Table 3. Fitted parameters of the electrical resistivity of the LCMO:xZnO composites with $x = 0$–0.475 with the correlated polaron hopping model described in the text. Here A/n is a constant, n is the density of charge carriers, T_{ca} is the charge order temperature, ε_p is the small polaron stabilization energy. k, c and c' are the coefficients which take care of the spin–spin scattering, short range atomic order and magnetic scattering, respectively, in the metallic regime and U_0 is the polaron hopping activation energy.

x	A/n (10^{-3} Ω cm K^{-1})	n (10^{17} cm^{-3})	T_{ca} (K)	ε_p (K)	U_0 (K)	θ	k
0.0	0.6	13.7	265	264	420	54	1.3
0.05	1.8	4.6	265	360	465	100	1.6
0.10	4.8	1.7	265	454	700	100	2.0
0.13	6.0	1.4	265	480	700	70	2.8
0.20	0.2	41.1	270	494	625	100	2.7
0.30	0.7	11.7	270	430	625	100	2.5
0.45	1.0	8.2	270	420	625	100	2.1
0.475	7.3	1.1	270	440	625	100	2.7

with

$$A = \frac{1.13k_B}{\nu_{ph}a^2e^2}, \tag{9}$$

where n is the density of charge carriers, ν_{ph} is the frequency of the longitudinal optical phonon mode to which the electron with charge e is coupled, a is the hopping distance and $m(t)$ $(=M(T)/M(0))$ is the normalized magnetization at the normalized temperature, t $(=T/T_{MI})$. Here T_{MI} is the temperature at which the peak resistivity occurs (this temperature is different from the magnetic transition temperature, T_C), σ_a is the short range order parameter, ε_p is the small polaron stabilization energy and U is the activation energy of the charge carriers, $U = U_0\xi^2$, where $\xi^2 = S_a^2(1 - S_m)^2\,\sigma_a^2$. Here U_0 is a constant, S_a is the long-range atomic order parameter and S_m is the long-range magnetic order parameter. To fit our resistivity data, we have used $S_a^2 = 1$, $\sigma_a^2 = (1 - ct_{ca}^3)^{1/2}$ and $(1 - S_m)^2 = (1 - m^k)$, where k is a variable related to spin–spin scattering and dependent on the compositions (x). Here $t_{ca} = T/T_{ca}$, where T_{ca} is the charge-order temperature [25] and m is obtained by solving $m = \tanh(m/t)$, appropriate for a system which has two stable spin states, $S_z = \pm S$. Since $m = \tanh(m/t)$ is valid only for $S = 1/2$, the method used represents an approximation only. In equation (9) we have taken $\nu_{ph} = 5 \times 10^{12}$ Hz and 'a' =3.85 Å. The θ added to T in the cosh term, compared to the original equation discussed in [25], is to take care of the zero point vibration of the atoms which prevent the complete localization of the polarons as $T \to 0$. The coefficient 'c' appears in the expression for σ_a related to short range atomic order while 'c'' relates to the magnetic scattering in the metallic regime and appears in equation (8). The values have been taken as $c = 0.70$ and 0.85 for pure LCMO ($x = 0$). These coefficients for the other composites ($0.05 \leqslant x \leqslant 0.475$) have been taken as 0.56 and 0.05, respectively, to fit the resistivity data. The other parameters used to fit the resistivity data are given in table 3 and the fit to the experimental resistivity data for the composites is shown in figures 9(a)–(f). In each case, there is a good fit with theory for $\rho(T)$ in the range 20 K to T_C. The localization expected for $T < 20$ K in the actual system is not as sharp as predicted by the theory, though in each case there is an indication of the upturn of the curve. In the paramagnetic regime, for $T > T_{MI}$, there is a small deviation from theory which may be due to short range spin order.

Using equations (8) and (9), and the parameters given in table 3, we have obtained the charge carrier density, n. We have plotted the variation of n with composition in figure 10. The charge carrier concentration (n) decreases from 13.7×10^{17} cm^{-3} for $x = 0.0$ to 1.4×10^{17} cm^{-3} for $x = 0.13$. This reduction of carrier concentration leads to a one order

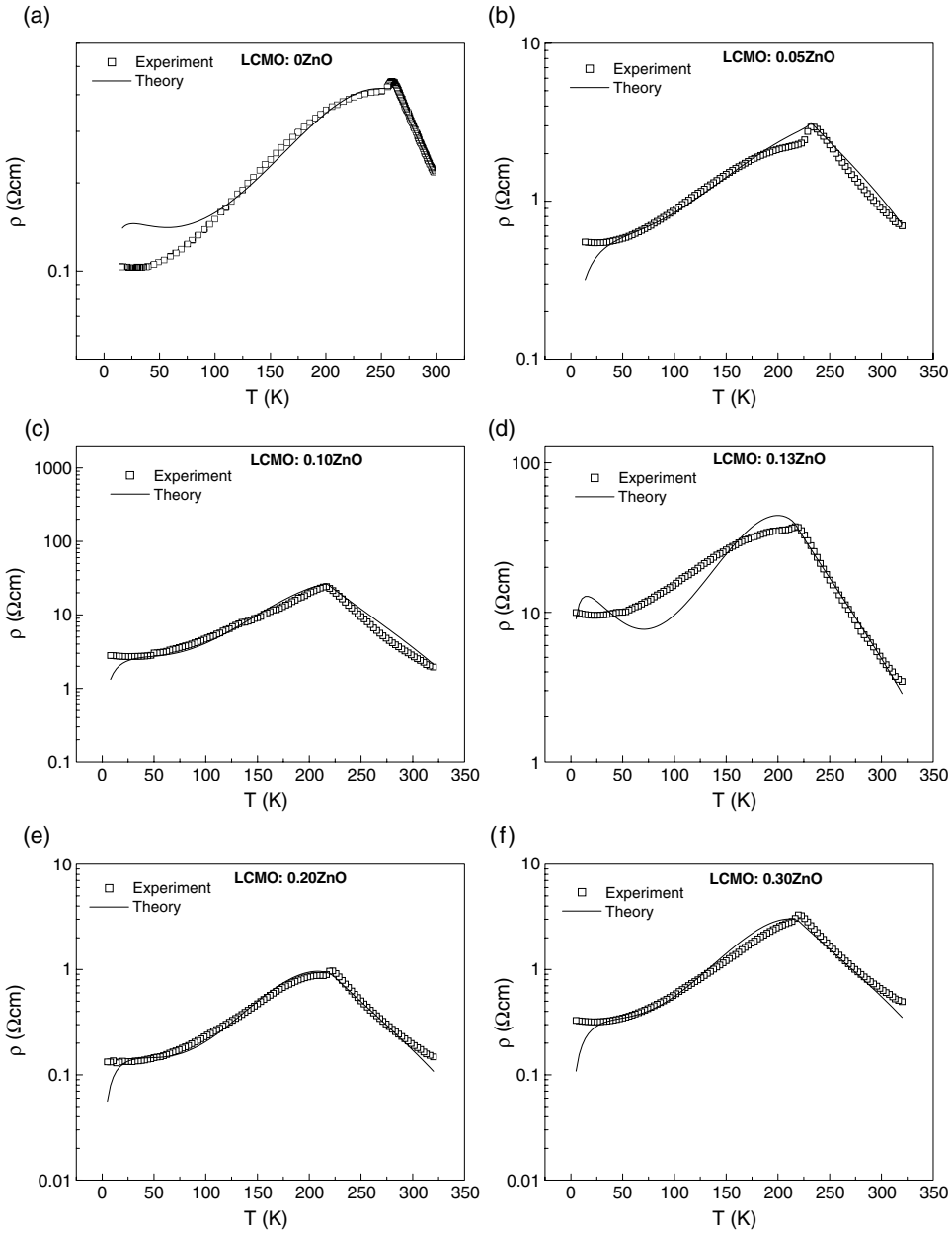

Figure 9. Fit of the experimental resistivity data with equation (8) discussed in the text for LCMO:xZnO samples with (a) $x = 0.0$, (b) $x = 0.05$, (c) $x = 0.10$, (d) $x = 0.13$, (e) $x = 0.20$, (f) $x = 0.30$, (g) $x = 0.45$ and (h) $x = 0.475$.

of magnitude increase in room temperature resistivity and two orders of magnitude increase in peak resistivity for $x = 0.13$. For lower values of x ($\leqslant 0.13$), Zn mostly goes into the lattice in the Mn site, reducing the mobility of the charge carriers (since DE is hindered) and segregates in a lesser amount in the grain boundary region, while for higher values of x, ZnO mostly segregates at the grain boundary. Consequently, formation of a percolation path for the

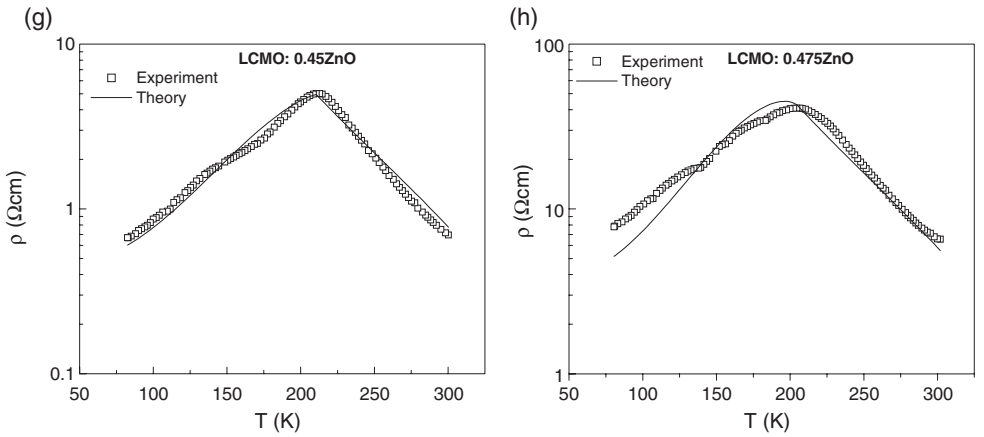

Figure 9. (Continued.)

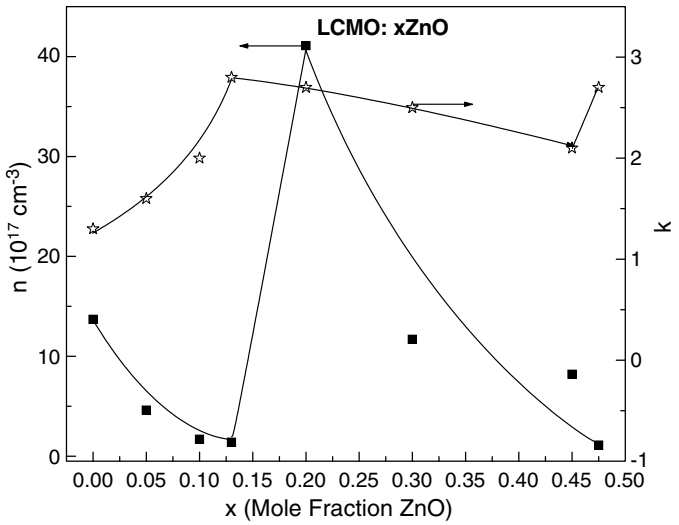

Figure 10. Variation of the charge carrier density (n) and spin–spin scattering coefficient, k, with composition (x) of LCMO:xZnO composites.

conducting LCMO with a smaller amount of Zn in the host matrix leads to an improvement in conductivity for $x > 0.13$ (figure 6). The spin–spin scattering term, which is related to the exponent k of m in equation (8) and is associated with the long range magnetic order parameter, S_m, follows the reverse trend to that of 'n' and is shown in figure 10. Xia *et al* [26, 27] have observed a similar effect in their YSZ doped LSMO and LCMO samples, respectively.

4. Conclusions

For the $La_{0.67}Ca_{0.33}MnO_3$:xZnO composites studied, Zn^{2+} mostly go into the perovskite lattice of LCMO if $x \leqslant 0.13$. But beyond this value of x, ZnO mainly segregates as a separate phase in the grain boundary region, improving the conductivity of the system. The overall transport behaviour of the system is described as a parallel combination of the low resistive intragrain

conduction and high resistive intergrain conduction. Using the same model, the grain and grain boundary contribution to the total resistivity is separated out for all the composites. The field dependent resistivity at 80 kOe shows that all the composites have higher value of MR compared to those in pure LCMO close to the transition temperatures and is a maximum of 76.6% for $x = 0.10$ at T_{MI}. All the composites show high low field MR at 8 kOe compared to pure LCMO, and is highest at about 29% for $x = 0.05$. The experimental resistivity data for all the composites shows a good agreement with the correlated polaron hopping model throughout the temperature range.

Acknowledgments

Part of the work, carried out at IIT Bombay, was supported by the Department of Science and Technology (DST), Government of India. We also acknowledge Saket Asthana for help in fitting the resistivity data.

References

[1] Rao C N R and Raveau B (ed) 1998 *Colossal Magnetoresistance, Charge Ordering and Related Properties of Manganese Oxides* (Singapore: World Scientific)
[2] Jin S, Tiefel T H, McCormack M, Fastnach R A, Ramesh R and Chen L H 1994 *Science* **264** 413
[3] Zener C 1951 *Phys. Rev.* **82** 403
[4] Hwang H Y, Cheong S W, Ong N P and Batlogg B 1996 *Phys. Rev. Lett.* **77** 2041
[5] Huang Y-H, Chen X, Wang Z-M, Liao C-S, Yan C-H, Zhao H-W and Shen B-G 2002 *J. Appl. Phys.* **91** 7733
[6] Shlyakhtin O A, Shin K H and Oh Y-J 2002 *J. Appl. Phys.* **91** 7403
[7] Balcells L I, Carrillo A E, Martinez B and Fontcuberta J 1999 *Appl. Phys. Lett.* **74** 4014
[8] Petrov D K, Krusin-Elbaum L, Sun J Z, Feild C and Duncombe P R 1999 *Appl. Phys. Lett.* **75** 995
[9] Köster S A, Moshnyaga V, Samwer K, Lebedev O I, Van Tendeloo G, Shapoval O and Belenchuk A 2002 *Appl. Phys. Lett.* **81** 1648
[10] Das D, Chowdhury P, Das R N, Srivastava C M, Nigam A K and Bahadur D 2002 *J. Magn. Magn. Mater.* **238** 178
[11] Das D, Saha A, Russek S E, Raj R and Bahadur D 2003 *J. Appl. Phys.* **93** 8301
[12] Huang Q, Li J, Huang X J, Ong C K and Gao X S 2001 *J. Appl. Phys.* **90** 2924
[13] Yan C-H, Xu Z-G, Zhu T, Wang Z-M, Cheng F-X, Huang Y-H and Liao C-S 2000 *J. Appl. Phys.* **87** 5588
[14] Yan C-H, Huang Y-H, Chen X, Liao C-S and Wang Z-M 2002 *J. Phys.: Condens. Matter* **14** 9607
[15] Gupta S, Ranjit R, Mitra C, Raychaudhuri P and Pinto R 2001 *Appl. Phys. Lett.* **78** 362
[16] Huang Y-H, Yan C-H, Luo F, Song W, Wang Z-M and Liao C-S 2002 *Appl. Phys. Lett.* **81** 76
[17] Tang T, Zhang S Y, Huang R S and Du Y W 2003 *J. Alloys Compounds* **353** 91
[18] Yan C-H, Luo F, Huang Y-H, Li X-H, Wang Z-M, Liao C-S, Zhao H-W and Shen B-G 2002 *J. Appl. Phys.* **91** 7406
[19] Liu J-M, Yuan G L, Sang H, Wu Z C, Chen X Y, Liu Z G, Du Y W, Huang Q and Ong C K 2001 *Appl. Phys. Lett.* **78** 1110
[20] Awana V P S, Schmitt E, Gmelin E, Gupta A, Sedky A, Narlikar A V, de Lima O F, Cardoso C A, Malik S K and Yelon W B 2000 *J. Appl. Phys.* **87** 5034
[21] Shim I-B, Bae S-Y, Oh Y-J and Choi S-Y 1998 *Solid State Ion.* **108** 241
[22] Ghosh K, Ogale S B, Ramesh R, Greene R L, Venkatesan T, Gapchup K M, Bathe R and Patil S I 1999 *Phys. Rev.* B **59** 533
[23] Gupta A, Gong G Q, Xiao G, Duncombe P R, Lecoeur P, Trouilloud P, Wang Y Y, Dravid V P and Sun J Z 1996 *Phys. Rev.* B **54** R15629
[24] Mahesh R, Mahendiran R, Raychaudhuri A K and Rao C N R 1996 *Appl. Phys. Lett.* **68** 2291
[25] Srivastava C M 1999 *J. Phys.: Condens. Matter* **11** 4539
[26] Xia Z C, Yuan S L, Zhang L J, Zhang G H, Feng W, Tang J, Liu L, Liu S, Liu J, Peng G, Li Z Y, Yang Y P, Tang C Q and Xiong C S 2003 *Solid State Commun.* **125** 571
[27] Xia Z C, Yuan S L, Tu F, Tang C Q, Peng G, Zhang G Q, Liu L, Liu J, Li Z Y, Yang Y P, Xiong C S and Xiong Y H 2002 *J. Phys. D: Appl. Phys.* **35** 177